Asian Journal of Chemistry; Vol. 37, No. 4 (2025), 925-930

ASIAN JOURNAL OF CHEMISTRY

https://doi.org/10.14233/ajchem.2025.33266

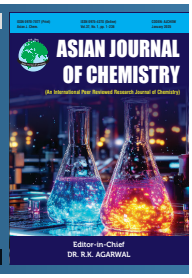

Facile Synthesis of Magnesium Oxide Nanoparticles for Effective Photocatalytic Degradation of Dyes

S. De[1,*] and B. Bhattacharjee[2]

[1]Department of Physics, Bankura Zilla Saradamani Mahila Mahavidyapith, Bankura-722101, India
[2]Department of Physics, Ramananda College, Bishnupur, Bankura-722122, India

*Corresponding author: E-mail: sanchita.de.pinki@gmail.com

Received: 20 December 2024; *Accepted*: 20 March 2025; *Published online*: 29 March 2025; AJC-21954

Significant environmental challenges require to be addressed to efficiently decompose the organic pollutants. Herein, a novel photocatalytic approach is proposed that leverages advanced nanomaterials to improve pollutant removal rates. The magnesium oxide nanoparticles were synthesized using simple chemical simultaneous precipitation method, utilizing magnesium nitrate as main precursor. The microstructural analysis of samples was investigated by XRD and SEM techniques. An absorption shifting toward the blue end of the spectrum observed in UV-VIS absorption spectrum suggests the development of MgO nanoparticles. Energy-gap energies of MgO nanoparticles were examined as function of calcination temperature and band-gap energies decreased from 5.43-5.04 eV, a change attributed to grain growth in samples. This finding aligns with the particle sizes determined from XRD and SEM. The typical sizes of the synthesized nanoparticles were ranged between 5-23 nm. The synthesized MgO nanoparticles demonstrated remarkable light-activated catalytic efficiency for the reduction of methyl orange and Victoria blue dyes under UV light exposure. Based on the results, a large number of native defects is associated with the excellent photocatalytic performance of synthesized MgO nanoparticles.

Keywords: Magnesium oxide, Photocatalytic degradation, Electrocatalysis, Methyl orange, Victoria blue.

INTRODUCTION

Nanotechnology offers promising advancements and serves as a foundation for sustaining research across several domains. It is described as a methodology focused on the preparation and profiling, development of utilizations using materials possessing a minimum of one dimension at the nanometer range [1]. Magnesium oxide nanoparticles have been found to be gaining greater emphasis than others commonly used nanoparticles composed of metal oxides, across various fields [2-4]. The biocompatibility, lightweight, multifunctionality, recyclability, non-toxicity and moisture sensitivity of these structural components make them attractive for use in biocompatible implant applications. These qualities significantly enhance their utility and additional attributes for example a elevated melting temperature, low-cost manufacture, biological decomposition ability and compatibility with biological systems, make nano-sized MgO particles highly versatile [5-8]. Furthermore, MgO NPs are significant because of their unique properties compared to bulk materials. Their exceptional characteristics set them apart from other substances. These include remarkable chemical resilience, excellent heat conductivity, minimal light bending coefficient and reduced electrical permittivity, high photocatalytic action or performance, elevated electrical susceptibility and environmental eco-friendly [9].

With the growing alongside the uses of different nanoparticles of metal oxides, MgO nanoparticles have also attracted significant consideration and are increasingly utilized because of their distinctive and unmatched characteristics. Magnesium oxide nanoparticles are straightforward to produce, pose no toxicity and cost effective. MgO nanoparticles possess a broad array of applications across industrial and biotechnological fields, including roles in bone regeneration, as antimicrobial agents and in treating cryoinjury [10-12]. Additionally, they are utilized in uranium ion sorption, catalysis, lithium-ion batteries and toxic waste management [13]. Due to their highly corrosive nature, the use of these nanoparticles in automotive and aerospace fields was initially limited. However, techniques like plating and conversion coating have reintroduced this material into these industries [14,15]. They are also well known for their antibacterial properties and antimicrobial activity [16-19].

Various commercial sectors, including textiles, paper manufacturing and food processing, employ aromatic compounds that readily disperse in water, leading to environmental pollution [20]. The waste from various industries and factories is often discharged into water bodies, containing dangerous substances in the form of metallic toxins. The majority of colourant wastes consist of persistent and non-decomposable azo dyes, that can have drastic harmful effects on both human and marine eco-systems due to their cancerous properties [21]. The high degree of stability and intricate arrangement of these dyes render conventional wastewater treatment techniques inadequate and inefficient. Therefore, use of metal oxides functioning as semiconductors photocatalysts for the entire removal of various harmful contaminants in nature has proven to be highly effective over the years [22].

Semiconductor photocatalysis is an advanced and highly effective method for wastewater remediation, providing the significant advantage of utilizing abundant natural sunlight. This approach is primarily leveraged for the development, analysis and exploration the photocatalytic properties of nanostructure materials, with a particular focus on their morphology and size [23]. For example, nanostructure materials like metallic nano-sized particles, metal oxide with porous structures, carbon nonmaterial and their integrated structures have been widely examined for possible uses in energy conversion, energy storage and gas storage systems, photocatalysis and electrocatalysis [24,25]. In the course of time, various metal based oxide nonmaterial like TiO_2, ZnO, CdO, Bi_2O_3 and CuO [26-29], along with graphitic non-material, have been utilized as effective photocatalysts for the breakdown of natural contaminants in aquatic and atmospheric environments [30,31]. In recent years, a shift has occurred significant global a growing interest has emerged in the photocatalytic breakdown of harmful organic pollutants has garnered attention. Specifically, the effluents containing coloured dyes generated by the textile and paper sectors are highly hazardous and resistant to biodegradation. Approximately 65-70% of these coloured dye wastewater consist of azo-based dyes, which contribute to significant environmental contamination through the release of toxic and potentially cancer causing substances into water systems [32].

The research on the photodegradation of synthetic colourants through the application of MgO nanoparticles is limited [33,34]. Within this study, the synthesis of MgO nanoparticles using an easy chemical co-precipitation technique is presented. TheMgO nanoparticles were characterized and conducted the photocatalytic activity of negatively charged dye, methyl orange dye (MO) and positively charged dye, Victoria blue (VB) under UV light irradiation.

EXPERIMENTAL

Synthesis of MgO nanoparticles: In a typical experimental procedure, 0.4 M of $MgNO_3 \cdot 6H_2O$ as precursor dissolved in 200 mL of distilled water was mixed with 0.6 M NaOH solution dropwise while swirling constant which results in the formation of milky-white solid residue and the agitation was constantly done for an additional 30 min. The solid residue was precipitated, washed and rinsed with methanol two-three times to eliminate ion-based contaminants. The precipitate was spunned at high speed in a centrifuge at 3000 rpm for 10 min and then dried at ambient temperature. The dried white powder samples were then calcined in air for 1 h at 250 ºC, 350 ºC and 500 ºC. The synthesized MgO nanoparticles calcined at 250, 350 and 500 ºC were labeled as samples 1, 3 and 6, respectively.

Characterization: A dual-beam UV-vis spectrophotometer (Model: Systronics AU-2703) was used to study the optical absorption. The morphological analysis was conducted using SEM (Make: ZEISS) at 5 kV accelerating voltages. The crystal form and stages were analyzed by X-ray powder diffraction (XRD) with Cu*K*α radiation (λ = 1.54178 Å) over a Bragg angle range of 30º to 80º.

Photocatalytic activity: The photocatalytic potential of synthesized MgO nanoparticles for dye degradation was evaluated by employing methyl orange (MO) and Victoria blue (VB) dyes with the ultraviolet exposure to light-ray (10 W, 30 mW/cm^2). Initially, a solution containing 100 mL of 15 mg/L MO and 5 mg, 10 mg, 15 mg of MgO nanoparticles (S-1, S-3, S-6) were, respectively stirred continuously for 10 min to establish equilibrium between adsorption and desorption. Similarly, 10 mg/L VB and 5 mg, 10 mg, 15 mg of MgO nanoparticles (S-1, S-3, S-6) were, respectively stirred for 10 min. At regular intervals, 10 mL of this mixture was collected then analyzed using UV-vis spectrophotometry to measure the dye concentration in that reaction solution. The percentage of degradation was analyzed using the following equation of methyl orange and Victoria blue dyes [35]:

$$\text{Degradation (\%)} = \frac{Z_o - Z_t}{Z_o} \times 100$$

where $Z_0 - Z_t$ represents the change in dye concentration from the initial to final value at its peak wavelength, while Z_0 represents the initial amount of colourant present prior to the reaction starts [36].

RESULTS AND DISCUSSION

UV-Vis spectral studies: The formation of MgO nanoparticles was confirmed through a strong absorption band observed at 215-225 nm is assigned to the MgO nanoparticles [37]. The absorption peak observed at 215 nm for sample S-1, 225 nm for sample S-3, and 224 nm for sample S-6 corresponds to the excitation of O^{2-} anions, which are four-fold coordinated at the boundaries and vertices. The band gap energy was calculated by utilizing Tauc plot and found to be 5.04 eV–5.43 eV [38] (Fig. 1).

XRD analysis: In X-ray powder diffraction (XRD), the diffraction peak of the synthesized MgO nanoparticles, following the total decrease of Mg^{2+} as shown in Fig. 2. The resulting XRD diffraction patterns were analyzed 2θ data in the 20º to 80º range using Cu*K*α radiation with a wavelength of λ = 1.5406 Å. A cubic structure aligns well with JCPDS card No. #721427 and JCPDS card No. 36-1451, confirmed the formation of MgO nanoparticles. Size of the particle was measured with the help of Debye-Scherrer (D-S) equation [39].

$$D_{MgO} = \frac{k\lambda}{\beta \cos\theta}$$

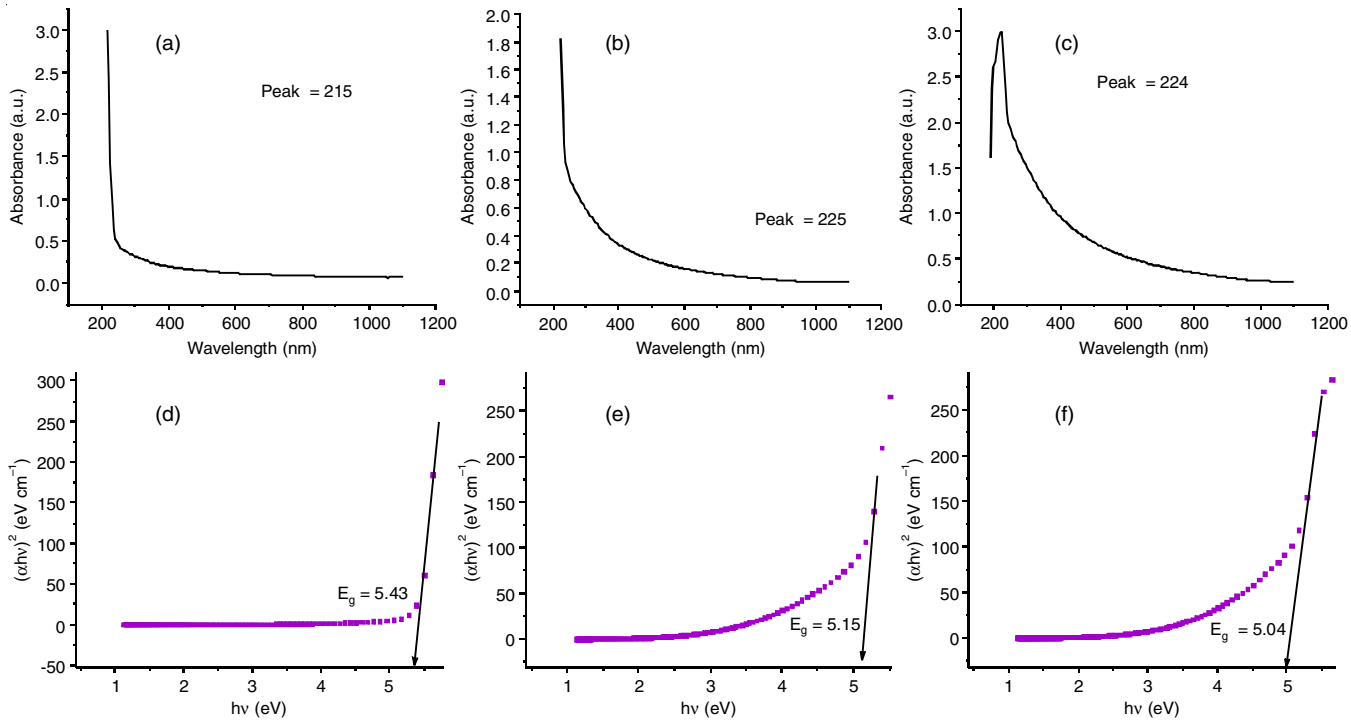

Fig. 1. (a-c) UV DRS of S-1, S-3, S-6 MgO nanoparticles and (d-f) plot of $(\alpha h\nu)^2$ *vs.* (hν) for S-1, S-3, S-6 MgO nanoparticles, respectively

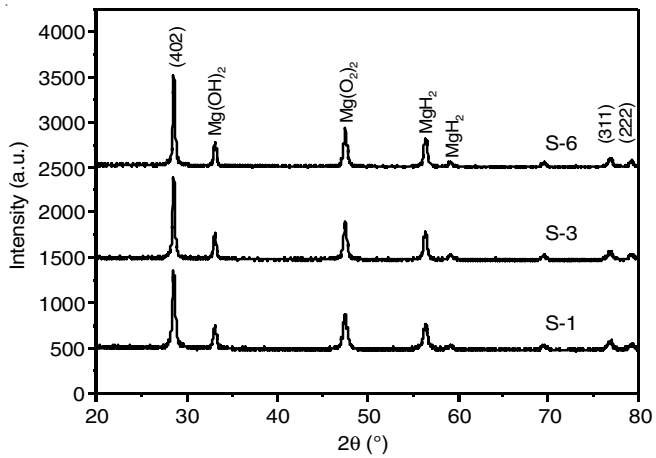

Fig. 2. XRD pattern of magnesium oxide (MgO) nanoparticles

where D_{MgO} represents the crystallite size; K is the shape factor (0.94); λ represents the X-ray wavelength (1.5402 Å) and β denotes the full width at half maximum (FWHM) of the diffraction peak. Based on the Scherrer equation, the typical crystal value of this synthesized MgO NPs, identify originating corresponding peaks, was determined and given in Table-1.

The Williamson-Hall (W-H) equation was also employed to calculate the crystallite grain size (D_{MgO}) of the nanocrystal, as described by the following equation:

$$\beta\cos\theta = 4\varepsilon\sin\theta + \frac{k\lambda}{D_{MgO}}$$

The computed values of various crystal parameters are shown in Table-1.

SEM studies: Fig. 3 shows the SEM images of synthesized MgO nanoparticles at different magnifications and revealed the presence of large-scale flower-like structures, which was formed due to the clumping of thin sheets [40]. These thin sheets were merged to form a 3-D network of MgO flower-like structures, resulting in large pores that could enhance the absorption mechanism by facilitating access to internal surface sites [41]. Even though the particles are adhered to one another, no actual bond is formed between them. This allows each particle to retain its distinct shape, characteristics and structure. These particles may undergo aggregation, where they come into close physical proximity without forming chemical bonds. The ImageJ software was used to calculate the average nanoparticle size, which found out to be 8-22 nm.

Photocatalytic activity: Under UV-visible light, the degradation of methyl orange (MO) and Victoria blue (VB) dyes was examined over a different interval of time periods. The MO and VB dyes have peak UV-visible absorption wavelengths of 464 nm and 615 nm, respectively. Fig. 4 illustrates the photodecomposition properties of MO and VB dyes with involvement

TABLE-1
STRUCTURAL CHARACTERISTICS AND OPTICAL ENERGY BAND-GAP OF MAGNESIUM OXIDE NANOPARTICLE

Sample code	Lattice constant (Å)	Crystallite size (nm)			Band gap (eV)
		D-S method	W-H method	Micro structural comparison (SEM analysis)	
S-1	4.248	8	5	6	5.43
S-3	4.276	15	11	8	5.15
S-6	4.251	22	19	22	5.04

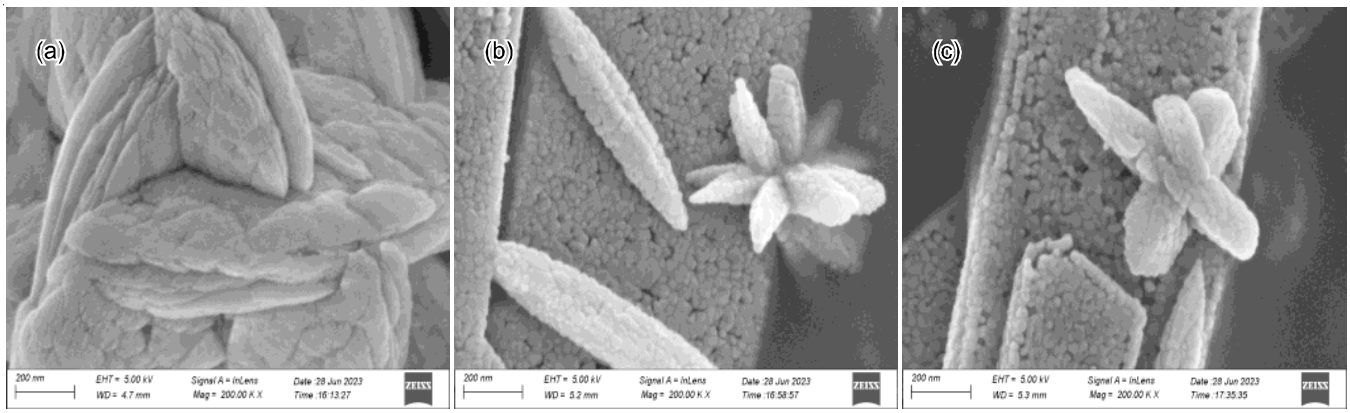

Fig. 3. SEM image of magnesium oxide (MgO) nanoparticles (a) S-1 (b) S-3 (c) S-6

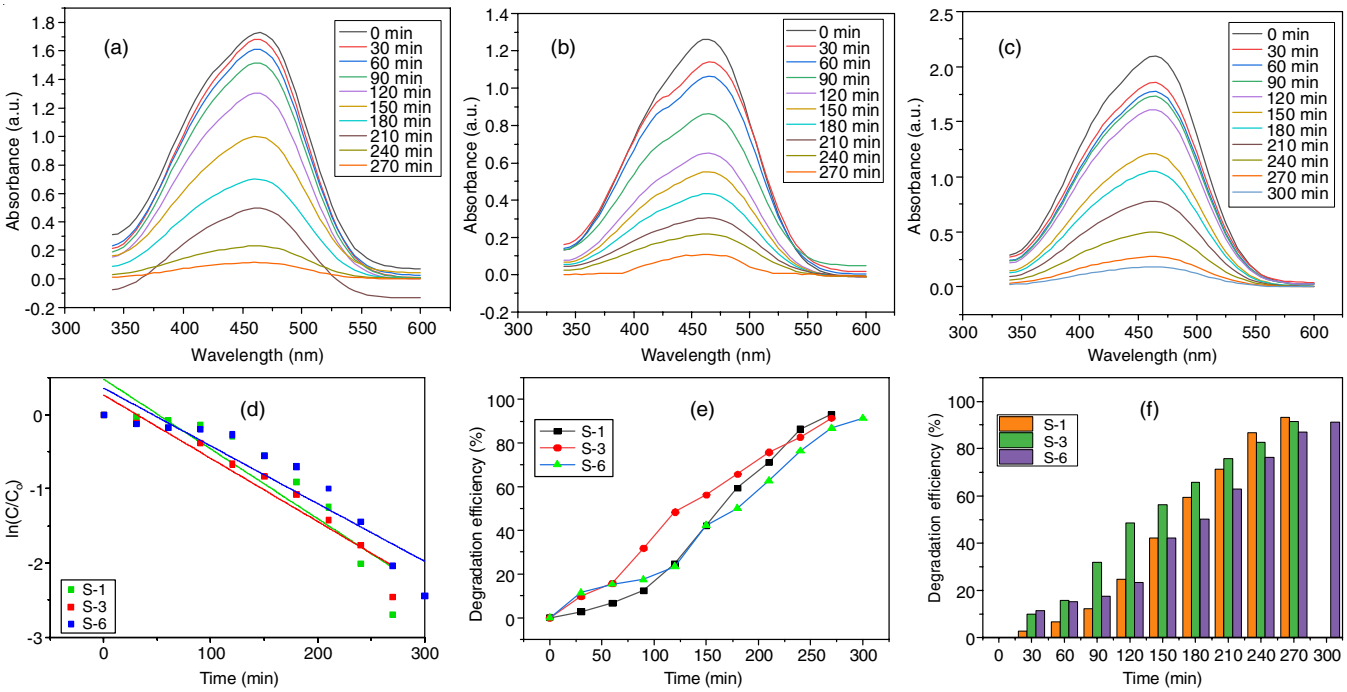

Fig. 4. Time-dependent absorption spectra curves of methyl orange dye solution with (a) S-1, (b) S-3 and (c) S-6; comparison of (d) degradation kinetics and (e), (f) degradation rate of methyl orange dye under varying conditions

of S-1, S-3 and S-6. The potential of synthesized MgO nanoparticles maximum absorbance at 464 nm for MO and 615 nm for VB decreased as exposure time increased, indicating a photocatalytic dye breakdown process. In presence of S-1, S-3 and S-6, the MO solution becomes completely colourless after 270 min, 270 min and 300 min of exposure to radiation, in the same order, while the VB dye becomes colourless following 120 min, signifying the full breakdown of dye compounds by MgO nanoparticles. The degradation efficiencies of S-1, S-3 and S-6 for MO dye were measured at 93%,91.5% and 91%, (Fig. 4e-f) respectively whereas the degradation efficiencies of S-1, S-3 and S-6 for VB dye were found to be 97%, 96% and 95 %, respectively (Fig. 5e-f). The enhanced degradation efficiency of S-1 for both MO and VB dyes signifies its superior photocatalytic ability. The improved degrading efficacy of S-1 can be attributed to its tiny crystallite structure, which enhances the surface area-to-volume ratio of the catalytic agents, leading to a higher number of active sites and surface hydroxyl groups [42]. Therefore, a large ratio of surface expanse to volume can enhance interaction between photocatalyst and the dye particles, leading to increased effectiveness of degradation.

Furthermore, the absorbance analysis were employed to analyze the rate of decomposition reaction utilizing the approximate first-order kinetic equation [43].

$$\ln\frac{Z_o}{Z} = Kt$$

Figs. 4d and 5d illustrate the plotting of the logarithm to the base of the ratio of concentration [Ln (Z_o/Z)] against exposure time to radiation for MO and VB dyes, in the corresponding order. The concentration levels on a logarithmic scale change proportionally over time, indicating that the photodegradation of MO and VB dyes follows first-order reaction kinetics. The reaction variables, including the degradation rate constant (K_r),

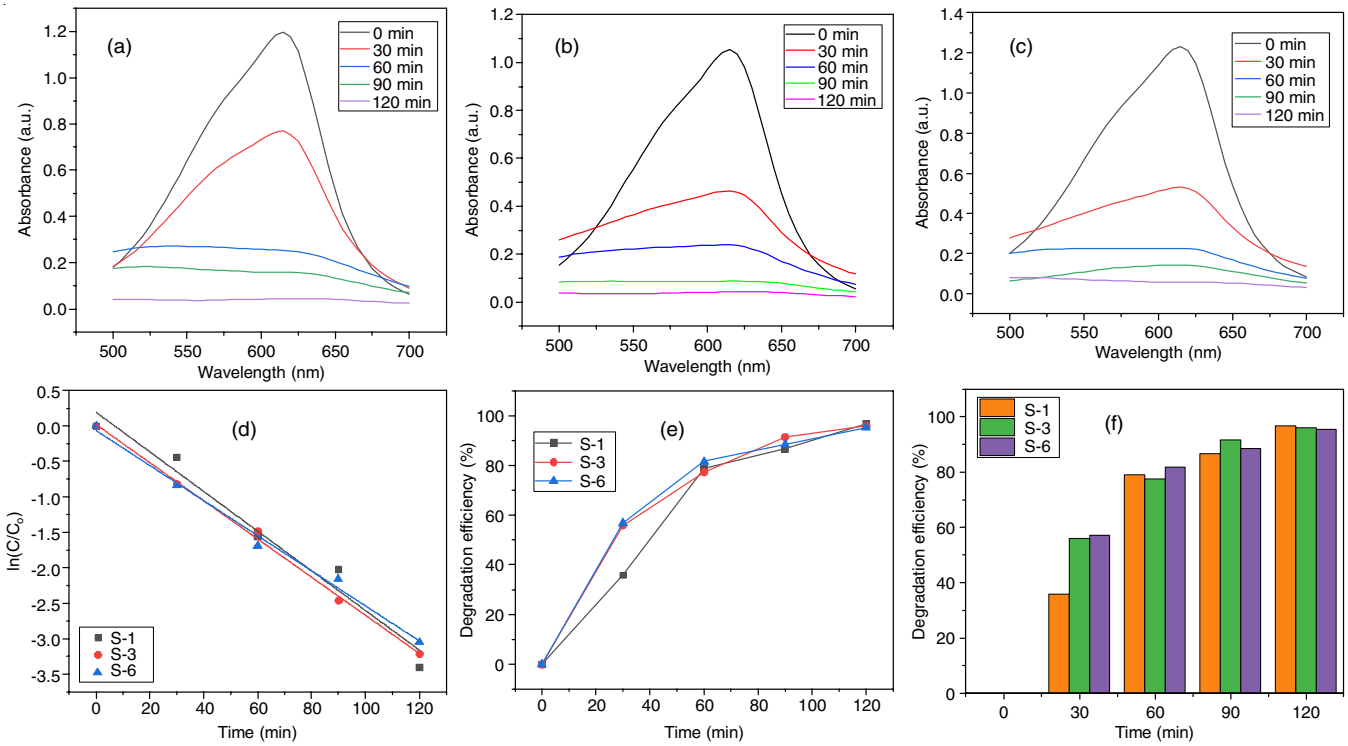

Fig. 5. Time-dependent absorption spectra curves of Victoria blue dye solution with (a) S-1, (b) S-3 and (c) S-6; comparison of (d) degradation kinetics and (e), (f) degradation rate of Victoria blue dye under varying conditions

half-life durations ($t_{½}$) and linear coefficient (R^2), derived from kinetics plots for MO and VB dyes, are presented in Table-2, which clearly demonstrates that S-1 possesses a higher rate constant and shorter ($t_{½}$) values compared to S-3 and S-6 for both MO and VB dyes, emphasizing the superior photocatalytic performance of S-1. The variation in degradation rates between the two dyes can be attributed to their structures and physicochemical characteristics, such as molecular dimension [44]. As the molecular structure of VB (458.05 g/mol) is significantly larger than that of MO (327.340 g/mol), so it requires a longer duration of exposure for total degradation of VB dye. In comparison with earlier study on MgO in photocatalysis, which revealed that VB dye degrades at 88% [45] and MO dye at 90% [46], this study highlights effective VB and MO degradation efficiencies of 97% and 93%, respectively.

Conclusion

In this work, an enhanced light-driven catalytic performance of flake-like MgO nanoparticles synthesized by chemical co-precipitation method is investigated. The existance of the uniform phase, box-shaped MgO nanoparticles with a flake-like structure and high levels of inherent defects was characterized by the XRD, SEM and UV-DRS techniques. The MgO nanoparticles synthesized in the optimal conditions were employed to break down methyl orange (MO) and Victoria blue (VB) dyes *via* photocatalysis. The results confirmed the typical decrease in the absorption curve of MO and VB dyes during degradation process. The reaction rates demonstrated that the first-order rate equation yielded the best fit, as evidenced by the R^2 value. Furthermore, it was employed to examine the influence of dye concentration and catalyst concentration on the percentage of degradation. The results indicate that the produced MgO nanoparticles are a viable choice for the efficient photocatalytic degradation of MO and VB dyes.

ACKNOWLEDGEMENTS

The author extends their sincere gratitute to the managements of Bankura Zilla Saradamani Mahila Mahavidyapith and Ramananda College, Bishnupur, Bankura, India. The authors also like to acknowledge the Coordinator, Centre of Excellence in Advanced Materials, National Institute of Technology, Durgapur, India for the microstructural characterization of the nonmaterial samples.

CONFLICT OF INTEREST

The authors declare that there is no conflict of interests regarding the publication of this article.

TABLE-2
KINETIC VARIABLES OF MgO NANOPARTICLES FOR THE DEGRADATION OF METHYL ORANGE AND VICTORIA BLUE DYES

Sample code	Methyl orange			Victoria blue		
	Rate const.	$t_{1/2}$	R^2	Rate const.	$t_{1/2}$	R^2
S-1	0.01	69.31	0.84218	0.02792	24.82	0.96794
S-3	0.00852	81.35	0.93465	0.02687	25.79	0.99735
S-6	0.00778	89.09	0.87174	0.02471	28.04	0.99212

REFERENCES

1. S. Malik, K. Muhammad and Y. Waheed, *Molecules*, **28**, 661 (2023); https://doi.org/10.3390/molecules28020661
2. H.C.S. Perera, V. Gurunanthanan, A. Singh, M.M.M.G.P.G. Mantilaka, G. Das and S. Arya, *J. Magnesium Alloys*, **12**, 1709 (2024); https://doi.org/10.1016/j.jma.2024.05.003
3. M.-A. Gatou, E. Skylla, P. Dourou, N. Pippa, M. Gazouli, N. Lagopati and E.A. Pavlatou, *Crystals*, **14**, 215 (2024); https://doi.org/10.3390/cryst14030215
4. M. Fernandes, K.R.B. Singh, T. Sarkar, P. Singh and R.P. Singh, *Adv. Mater. Lett*., **11**, 20081543 (2020); https://doi.org/10.5185/amlett.2020.081543
5. K. Vijai Anand, A.R. Anugraga, M. Kannan, G. Singaravelu and K. Govindaraju, *Mater. Lett*., **271**, 127792 (2020); https://doi.org/10.1016/j.matlet.2020.127792
6. S.K. Verma, K. Nisha, P.K. Panda, P. Patel, P. Kumari, M.A. Mallick, B. Sarkar and B. Das, *Sci. Total Environ*., **713**, 136521 (2020); https://doi.org/10.1016/j.scitotenv.2020.136521
7. V. Nishchay, P. Krishna, K.S. Amit and B. Amit, *Mater. Technol*., **37**, 706 (2022); https://doi.org/10.1080/10667857.2021.1873634
8. A. Khalid, R. Norello, A.N. Abraham, J.-P. Tetienne, T.J. Karle, E.W.C. Lui, K. Xia, P.A. Tran, A.J. O'Connor, B.G. Mann, R. de Boer, Y. He, A.M.C. Ng, A.B. Djurisic, R. Shukla and S. Tomljenovic-Hanic, *Nanomaterials*, **9**, 1360 (2019); https://doi.org/10.3390/nano9101360
9. E. Saied, A.M. Eid, S.E. Hassan, S.S. Salem, A.A. Radwan, M. Halawa, F.M. Saleh, H.A. Saad, E.M. Saied and A. Fouda, *Catalysts*, **11**, 821 (2021); https://doi.org/10.3390/catal11070821
10. M. Vergheese and S.K. Vishal, *J. Pharmacogn. Phytochem.*, **7**, 1193 (2018).
11. J. Suresh, G. Pradheesh, V. Alexramani, M. Sundrarajan and S.I. Hong, *Adv. Powder Technol.*, **29**, 1685 (2018); https://doi.org/10.1016/j.apt.2018.04.003
12. M.V. Ratnam, C. Karthikeyan, K.N. Rao and V. Meena, *Mater. Today Proc.*, **26**, 2308 (2020); https://doi.org/10.1016/j.matpr.2020.02.498
13. J.-H. Shim, S. Lee and S.S. Park, *Chem. Mater.*, **26**, 2537 (2014); https://doi.org/10.1021/cm403846a
14. A.S. Gnedenkov, S.L. Sinebryukhov, D.V. Mashtalyar and S.V. Gnedenkov, *Corros. Sci.*, **102**, 269 (2016); https://doi.org/10.1016/j.corsci.2015.10.015.
15. M.M. Khin, A.S. Nair, V.J. Babu, R. Murugan and S. Ramakrishna, *Energy Environ. Sci.*, **5**, 8075 (2012); https://doi.org/10.1039/c2ee21818f
16. K. Karthik, S. Dhanuskodi, S. Prabu Kumar, C. Gobinath and S. Sivaramakrishnan, *Mater. Lett.*, **206**, 217 (2017); https://doi.org/10.1016/j.matlet.2017.07.004
17. H. Bhoi, P. Joshi, K. Punia, G. Lal and S. Kumar, *AIP Conf. Proc.*, **2220**, 020109 (2020); https://doi.org/10.1063/5.0001269
18. Z.T. Khodair, A.H. Abed and S.G. Majeed, *Eng. Technol.*, **3**, 43 (2016).
19. J.Y. Park, Y.J. Lee, K.W. Jun, J.O. Baeg and D.J. Yim, *J. Ind. Eng. Chem.*, **12**, 882 (2006).
20. S. Dervin, D.D. Dionysiou and S.C. Pillai, *Nanoscale*, **8**, 15115 (2016); https://doi.org/10.1039/C6NR04508A
21. K.-T. Chung, *J. Environ. Sci. Health, Part C*, **34**, 233 (2016); https://doi.org/10.1080/10590501.2016.1236602
22. J. Xie, H. Wang, M. Duan and L. Zhang, *Appl. Surf. Sci.*, **257**, 6358 (2011); https://doi.org/10.1016/j.apsusc.2011.01.105
23. S. Sharma, S.K. Mehta and S.K. Kansal, *J. Alloys Compd.*, **699**, 323 (2017); https://doi.org/10.1016/j.jallcom.2016.12.408
24. S. Kaur, S. Sharma and S.K. Kansal, *Superlattices Microstruct.*, **98**, 86 (2016); https://doi.org/10.1016/j.spmi.2016.08.011
25. S. Sood, S.K. Mehta, A. Umar and S.K. Kansal, *New J. Chem.*, **38**, 3127 (2014); https://doi.org/10.1039/C4NJ00179F
26. S. Sharma, S.K. Mehta, A.O. Ibhadon and S.K. Kansal, *J. Colloid Interface Sci.*, **533**, 227 (2019); https://doi.org/10.1016/j.jcis.2018.08.056
27. A. Kaur, A. Umar and S.K. Kansal, *J. Colloid Interface Sci.*, **459**, 257 (2015); https://doi.org/10.1016/j.jcis.2015.08.010
28. S. Sharma, A. Umar, S.K. Mehta and S.K. Kansal, *Ceram. Int.*, **43**, 7011 (2017); https://doi.org/10.1016/j.ceramint.2017.02.127
29. L. Zhang, P. Ma, L. Dai, S. Li, W. Yu and J. Guan, *Catal. Sci. Technol.*, **11**, 3834 (2021); https://doi.org/10.1039/D1CY00239B
30. G. Xu, L. Zhang, W. Yu, Z. Sun, J. Guan, J. Zhang, J. Lin, J. Zhou, J. Fan, V. Murugadoss and Z. Guo, *Nanotechnology*, **31**, 225402 (2020); https://doi.org/10.1088/1361-6528/ab76eb
31. L. Zhang, Q. Zhang, H. Xie, J. Guo, H. Lyu, Y. Li, Z. Sun, H. Wang and Z. Guo, *Appl. Catal. B*, **201**, 470 (2017); https://doi.org/10.1016/j.apcatb.2016.08.056
32. S.K. Kansal, N. Kaur and S. Singh, *Nanoscale Res. Lett.*, **4**, 709 (2009); https://doi.org/10.1007/s11671-009-9300-3
33. M.Y. Guo, A.M.C. Ng, F. Liu, A.B. Djurišic and W.K. Chan, *Appl. Catal. B*, **107**, 150 (2011); https://doi.org/10.1016/j.apcatb.2011.07.008
34. R. Wahab, S.G. Ansari, M.A. Dar, Y.S. Kim and H.S. Shin, *Mater. Sci. Forum*, **558-559**, 983 (2007); https://doi.org/10.4028/www.scientific.net/MSF.558-559.983
35. G.K. Sukhadeve, H. Bandewar, S.Y. Janbandhu, J.R. Jayaramaiah and R.S. Gedam, *J. Mol. Liq.*, **369**, 120948 (2023); https://doi.org/10.1016/j.molliq.2022.120948
36. S. Saman, A. Balouch, F.N. Talpur, A.A. Memon, B.M. Mousavi and F. Verpoort, *Appl. Organomet. Chem.*, **35**, e6199 (2021); https://doi.org/10.1002/aoc.6199
37. K. Mageshwari, S.S. Mali, R. Sathyamoorthy and P.S. Patil, *Powder Technol*., **249**, 456 (2013); https://doi.org/10.1016/j.powtec.2013.09.016
38. K.M. Rajeshwari, M.R. Suhasini, S. Bindya, A.B. Hemavathi, N. Ali, R.G. Amachawadi, C. Shivamallu, R.L.S. Hallurf, S.S. Majani and S.P. Kollur, *Results Chem.*, **6**, 101193 (2023); https://doi.org/10.1016/j.rechem.2023.101193
39. S.S. Majani, S. Sathyan, M.V. Manoj, N. Vinod, C. Shivamallu, K.N. Venkatachalaiah, S. Pradeep and S.P. Kollur, *Curr. Res. Green Sustain. Chem.*, **6**, 100367 (2023); https://doi.org/10.1016/j.crgsc.2023.100367
40. M. Chen, Y. Zhang, L. Xing, Y. Liao, Y. Qiu, S. Yang and W. Li, *Adv. Mater.*, **29**, 1607015 (2017); https://doi.org/10.1002/adma.201607015
41. S. Ahmed, H.U. Rehman, Z. Ali, A. Qadeer, A. Haseeb and Z. Ajmal *Surf. Interfaces*, **23**, 100953 (2021); https://doi.org/10.1016/j.surfin.2021.100953
42. G.K. Prasad, P.V.R.K. Ramacharyulu, B. Singh, K. Batra, A.R. Srivastava, K. Ganesan and R. Vijayaraghavan, *J. Mol. Catal. A Chemical*, **349**, 55 (2011); https://doi.org/10.1016/j.molcata.2011.08.018
43. X. Jiang, L. Yang, P. Liu, X. Li and J. Shen, *Colloids Surf. B Biointerfaces*, **79**, 69 (2010); https://doi.org/10.1016/j.colsurfb.2010.03.031
44. Y.L. Pang and A.Z. Abdullah, *Ultrason. Sonochem.*, **19**, 642 (2012); https://doi.org/10.1016/j.ultsonch.2011.09.007
45. S.A. Kumar, M. Jarvin, S. Sharma, A. Umar, S.S.R. Inbanathan and A.K. Nayak, *ES Food Agroforestry*, **5**, 14 (2021); https://doi.org/10.30919/esfaf519
46. M.R.R. Mofrad, G.R. Mostafaii, R. Nemati, H. Akbari and N. Hakimi, *Desalin. Water Treat*., **57**, 8330 (2016); https://doi.org/10.1080/19443994.2015.1017744